Wave-ice interactions in the marginal ice zone. Part 1: Theoretical foundations

Timothy D. Williams[a], Luke G. Bennetts[b], Vernon A. Squire[c], Dany Dumont[d], Laurent Bertino[a,e]

[a] *Nansen Environmental and Remote Sensing Center, Thormøhlensgate 47, 5006 Bergen, Norway*
[b] *School of Mathematical Sciences, North Terrace Campus, The University of Adelaide, SA 5005 Australia*
[c] *Department of Mathematics and Statistics, University of Otago, P.O. Box 56, Dunedin 9054, New Zealand*
[d] *Institut des sciences de la mer, Université du Québec à Rimouski, 310 allée des ursulines, C.P. 3300, Rimouski G5L 3A1 Québec, Canada*
[e] *Bjerknes Center for Climate Research, Bergen, Norway*

Abstract

A wave-ice interaction model for the marginal ice zone (MIZ) is reported that calculates the attenuation of ocean surface waves by sea ice and the concomitant breaking of the ice into smaller floes by the waves. Physical issues are highlighted that must be considered when ice breakage and wave attenuation are embedded in a numerical wave model or an ice/ocean model.

The theoretical foundations of the model are introduced in this paper, forming the first of a two-part series. The wave spectrum is transported through the ice-covered ocean according to the wave energy balance equation, which includes a term to parameterize the wave dissipation that arises from the presence of the ice cover. The rate of attenuation is calculated using a thin elastic plate scattering model and a probabilistic approach is used to derive a breaking criterion in terms of the significant strain. This determines if the local wave field is sufficient to break the ice cover. An estimate of the maximum allowable floe size when ice breakage occurs is used as a parameter in a floe size distribution model, and the MIZ is defined in the model as the area of broken ice cover. Key uncertainties in the model are discussed.

Email addresses: `timothy.williams@nersc.no` (Timothy D. Williams),

1. Introduction

Access to the seasonally ice-covered seas is increasing due to the impact of climate change (see, e.g., Stephenson et al., 2011) and commercial activities there are proliferating as a result. High precision forecasts of these regions are therefore in great demand. This paper and its companion (referred to as Part 2, Williams et al., submitted,) is a step towards making those forecasts as accurate as practicable, by including additional physics that is currently absent in today's ice/ocean models.

Improved spatial resolution has significantly enhanced how models represent the mean sea state and its variability, but it has also highlighted a number of problems that have previously remained hidden. One of them concerns the role of surface gravity waves in shaping the so-called marginal ice zone (MIZ), an important region between the open ocean and the interior pack ice where intense coupling between waves, sea ice, ocean and the atmosphere occurs. The MIZ is identified visually as a collection of relatively small floes. Surface waves are the main agent responsible for ice fragmentation and, depending upon wave and sea ice properties, they can propagate long distances into the ice field and still contribute to fracture. Indeed, Prinsenberg and Peterson (2011) recorded flexural failure induced by swell propagating within multiyear pack ice during the summer of 2009, even at very large distances from the ice edge in the Beaufort Sea. (Asplin et al., 2012, further analyzed this event.) While the local sea ice there qualified as being heavily decayed by melting (Barber et al., 2009), and thus more fragile, these observations suggest that such events could occur more frequently deep within the ice pack in a warmer Arctic that is no longer protected by a durable, extensive shield of sea ice.

Interactions between ocean waves and sea ice occur on small to medium scales, but they have a profound effect on the large-scale dynamics and thermodynamics of the sea ice. On a large scale the ice cover deforms in response to stresses imposed by winds and currents. It is customary to model pack ice as a uniform viscous-plastic (VP) material (Hibler, 1979; Hunke and Dukowicz, 1997), but alternatives such as the elasto-brittle rheology of Girard et al. (2010) have been proposed to account for the discrepancies in spatial and

luke.bennetts@adelaide.edu.au (Luke G. Bennetts), vernon.squire@otago.ac.nz (Vernon A. Squire), dany_dumont@uqar.ca (Dany Dumont), laurent.bertino@nersc.no (Laurent Bertino)

temporal scalings of ice deformations between VP model predictions and observations (Rampal et al., 2008; Girard et al., 2009). These models, however, function best when the sea ice is highly compact and sustains large internal stresses with deformation primarily along failure lines.

In contrast, floe sizes in the MIZ are generally smaller due to wave-induced ice breakage and the ice cover is therefore normally less compact, internal stresses are less important than other forcing because the ice floes are freer to move laterally, and deformations occur more fluently compared to the plastic-like, discontinuous deformation of the compact central ice pack. In this regime, internal stresses arise more from floe-floe contact forces than from any connate constitutive relation that embodies the behaviour of sea ice at large scales. Evidently, a model of the MIZ requires knowledge of how waves control the floe size distribution (FSD). Recognizing this, Shen et al. (1986) and Feltham (2005) have proposed granular-type rheologies for the MIZ that contain an explicit dependence on floe size, while others have presented direct numerical simulations of the MIZ using granular models with either a single floe diameter (e.g. Shen and Sankaran, 2004; Herman, 2011), or with floe diameters sampled from a power-law type FSD (Herman, 2013). Parameterizations for floe size-dependent thermodynamical processes have also been developed (Steele et al., 1989; Steele, 1992).

The distance over which waves induce the sea ice to break, i.e. the width of the MIZ, is controlled by exponential attenuation of the waves imposed by the presence of ice-cover. The rate of wave attenuation depends on wave period and the properties of the ice cover (Squire and Moore, 1980; Wadhams et al., 1988). Wave attenuation is modeled using multiple wave scattering theory or by models in which the ice cover is a viscous fluid or a viscoelastic material. In scattering models, wave energy is reduced with distance traveled into the ice-covered ocean by an accumulation of the partial reflections that occur when a wave encounters a floe edge (Bennetts and Squire, 2012b). Scattering models are hence strongly dependent on the FSD. In viscous models (e.g. Weber, 1987; Keller, 1998; Wang and Shen, 2011a) wave energy is lost to viscous dissipation, so these models are essentially independent of the FSD. We will use an attenuation model that includes both multiple wave scattering and viscous dissipation of wave energy. This means that there is a feedback between the FSD and wave attenuation, since the amount of breaking depends on how much incoming waves are attenuated, and the amount of scattering depends on how much breaking there is.

The notion and importance of integrating wave-ice interactions into an ice/ocean model is not new; indeed it was broached by the third author (VAS) more than two decades ago. Since then, several authors have presented numerical models for transporting wave energy into ice-covered fluids. Masson and LeBlond (1989) were the first to incorporate the effects of ice into the wave energy transport/balance equation that had previously been only used to model waves in open water (Gelci et al., 1957; Hasselmann, 1960; WAMDI Group, 1988; Ardhuin et al., 2010). Masson and LeBlond (1989) studied the evolution of the wave spectrum with time and distance into the ice and their theory was used subsequently by Perrie and Hu (1996) to compare the attenuation occurring in the ice field with experimental data. Meylan et al. (1997) derived a similar transport equation to that of Masson and LeBlond (1989) using the work of Howells (1960), and concentrated on the evolution of the directional spectrum. While, like us, they neglected non-linearity and the effects of wind and dissipation due to wave breaking, they improved the floe model by representing the ice as a thin elastic plate rather than as a rigid body. Doble and Bidlot (submitted) have also recently extended the operational wave model WAM into the ice in the Weddell Sea, Antarctica, using the attenuation model of Kohout and Meylan (2008). While this model does not allow for directional scattering, it does include the usual open-water sources of wave generation and dissipation in the same way that Masson and LeBlond (1989) and Perrie and Hu (1996) did.

The above papers give the framework and demonstrate some implementations of wave energy transport into the sea ice, but all neglect ice breakage. In fact, it is only recently that this effect was included by Dumont et al. (2011) (hereafter referred to as DKB) in a wave transport problem. Previous papers modeling ice fracture are those by Langhorne et al. (2001) and Vaughan and Squire (2011). However, those authors only looked at general properties of the ice cover, such as the lifetimes of ice sheets and the width of the MIZ. The method used involved modeling the attenuation of an incident wave spectrum and defining probabilistic breaking criteria to decide when the strains in the ice would exceed a breaking strain. The model of DKB provides a fuller description of the resulting ice cover: it estimates the spatial variation of floe sizes throughout the entire region where breaking occurs and also allows the temporal evolution to be investigated. In addition, it considers the coupling between the breaking and the transport of wave energy.

Although the DKB model is one-dimensional, i.e. it only considers a transect of the ocean, it is theoretically generalizable to include the second horizontal dimension. Before this geometrical restriction is tackled, however, important themes have been identified for discussion and investigation, which is the purpose of this paper. Firstly, we put the work of DKB into the context of previous work on modeling wave energy in ice (Masson and LeBlond, 1989; Perrie and Hu, 1996; Meylan and Masson, 2006) and we correct their interpretation of the spectral density function. Secondly, we revise the floe-breaking criteria based on monochromatic wave amplitudes employed by DKB, and propose one that is based on wave statistics instead. Numerical issues, sensitivity analyses and model results are reserved until Part 2.

2. Description of the waves-in-ice model

2.1. Overview

Figure B.1 shows the flow of information into and out of the waves-in-ice model (WIM), whose three components, namely advection, attenuation and ice breakage, are discussed in more detail in §3. We briefly describe their relationship to the inputs and outputs here.

The advection and attenuation steps depend on the group velocity, c_{g}, and the attenuation coefficient, $\hat{\alpha}$. Both c_{g} and $\hat{\alpha}$ depend on frequency in addition to the ice properties. The advection and attenuation steps describe how the wave energy is transported into the ice-covered ocean. The WIM therefore extends contemporary external wave models (EWMs, e.g. WAM, WAVEWATCH III), which typically do not operate in ice-covered oceans. The presence of waves in ice-covered oceans causes ice breakage to occur in the MIZ, thereby altering the local FSD.

The outputs will, of course, have follow-on effects on the ice properties when they are fed back into the ice-ocean model. For instance, we use the FSD to distinguish between interior pack ice and the MIZ. Consequently, the FSD determines which ice rheology applies to different areas and thus how the ice drifts. It can also be used to change the thermodynamics of the ice by increasing melting or freezing due to the extra surface area exposed to the air and water (Steele, 1992).

Another important follow-on/coupling effect is the momentum/energy exchange between the waves, the ocean and the atmosphere. Even without the complicating presence of sea ice, the question of how to couple ocean models to the wave field is not yet resolved (e.g. Babanin et al., 2009; Ardhuin et al., 2008). With attendant sea ice as well, wave attenuation occurs which we include in our model by considering two processes. Part of the energy lost by the waves as they travel into an ice field is attributed to scattering. In our model the scattering process is conservative and so energy lost in this way must be reflected back into the open ocean. The proportion of reflected energy can be calculated. The remaining energy loss is parameterized in the model by adding a damping pressure, which resists particle motion at the ice-water interface (see Appendix A). The actual mechanisms responsible for this energy loss are poorly understood and inadequately parameterized at present, and further investigation will be required to balance momentum/energy in a fully coupled model. Notwithstanding, it is important to include damping in the WIM to accurately predict the distance waves travel into the ice-covered ocean, and hence the region of ice broken by the waves, i.e. the width of the MIZ.

2.2. Inputs and outputs

The inputs to the WIM are the ice properties, the incident wave field and the initial FSD. Technically the FSD is also an ice property, but we treat it separately due to the special role it plays in the WIM.

The ice properties are all considered to vary spatially but not to vary in time. The ice concentration (c) and thickness (h) are standard variables of ice/ocean models, and so estimates for them can be easily obtained. However, the effective Young's modulus (Y^*), Poisson's ratio (ν) and breaking strain (ε_c) are non-standard and must be estimated (see §4.3). A value for the damping coefficient Γ, which is included to increase the attenuation of long waves as this is underpredicted by conservative scattering theory, is extracted from the attenuation measurements of Squire and Moore (1980) (see Appendix A and §4.2).

The wave energy is described by the spectral density function (SDF) $S(\omega, x, t)$, where $\omega = 2\pi/T$ is the angular frequency and T is the wave period. (For brevity, the SDF is sometimes written $S = S(\omega)$, taking the spatial (x) and temporal (t) dependencies to be implicit.) The wave spectrum may be defined either in the open ocean or within the sea ice, after having undergone some attenuation. However, most EWMs only predict S inside a region known as a wave mask, which currently stops at a conservative distance from the ice edge. If $x = 0$ is the edge of the wave mask, the EWM provides the initial boundary condition for the WIM, $S(\omega, 0, t) = S_0(\omega, t)$, where S_0 is known. The WIM advects this initial spectrum across the gap between the wave mask and the ice mask, and then into the ice-covered ocean.

The wave spectrum is advected according to the energy transport equations in §3.1—numerical details are given in Part 2.

The FSD is characterized by two spatially varying floe length parameters, $D_{\max}(x,t)$ and $\langle D\rangle(x,t)$, which also evolve with time. These are the maximum floe length and average floe length, respectively. The initial FSD is generally unknown. In our experiments we assume that prior to wave-induced ice breakage all floe lengths have a large value (e.g. 500 m; the precise value turns out to be relatively unimportant). After the waves have traveled into the ice and caused ice breakage, the FSD is parameterized as in §4.1

3. Model components

3.1. Advection and attenuation

The waves are advected according the energy balance equation, namely

$$\frac{1}{c_{\mathrm{g}}}D_t S(\omega;x,t) = R_{\mathrm{in}} - R_{\mathrm{ice}} - R_{\mathrm{other}} - R_{\mathrm{nl}}, \tag{1}$$

(Masson and LeBlond, 1989; Meylan and Masson, 2006; Ardhuin et al., 2010), where c_{g} is the group velocity and $D_t \equiv (\partial_t + c_{\mathrm{g}}\partial_x)$. The source terms R_{in}, R_{ice} and R_{other} represent respectively the wind energy input, rates of energy loss to (or due to) the ice and the total of all other dissipation sources (e.g. friction at the bottom of the sea, losses from wave breaking or white-capping, Ardhuin et al., 2010). These are all quasi-linear in S. The R_{nl} term incorporates fully non-linear energy exchanges between frequencies (Hasselmann, 1962, 1963).

For the WIM, we set $R_{\mathrm{other}} = R_{\mathrm{nl}} = 0$ and $R_{\mathrm{ice}} = \hat{\alpha}S$, i.e.

$$\frac{1}{c_{\mathrm{g}}}D_t S(\omega;x,t) = -\hat{\alpha}(\omega,c,h,\langle D\rangle)S(\omega;x,t). \tag{2}$$

The quantity $\hat{\alpha}$ is the dimensional attenuation coefficient, given by

$$\hat{\alpha} = \frac{\alpha c}{\langle D\rangle}, \tag{3}$$

where α is the non-dimensional attenuation coefficient, i.e. the (average) amount of attenuation per individual floe, which is a function of ice thickness and wave period. The definition $R_{\mathrm{ice}} = \hat{\alpha}S$ does not allow transfer of energy between directions (via diffraction by ice floes), as done by Masson and LeBlond (1989), Perrie and Hu (1996), and Meylan et al. (1997). This is a necessary limitation of the one-dimensional numerical model outlined in

Part 2. R_{ice} is quasi-linear since an S that is sufficiently large to cause breaking lowers the average floe size $\langle D \rangle$ and subsequently increases $\hat{\alpha}$, according to (3).

The effects of neglecting R_{other} and R_{nl} are not clear. They may be important in moving the energy across the gap between the wave and ice masks, although we note that as the resolution of the EWMs increases, this will become less of an issue. It is difficult to say how much effect these terms will have once the waves are in the ice-covered ocean, or how they should change to represent the different environment there. Masson and LeBlond (1989), Perrie and Hu (1996) and Doble and Bidlot (submitted) assumed some of the effects (like wind generation) were proportional to the open water fraction, and that R_{nl} was the same in the ice-covered ocean as in open water. (Polnikov and Lavrenov, 2007, recently confirmed the validity of this last assumption.) We note that by including wind generation in the ice, Perrie and Hu (1996) were able to reproduce (qualitatively at least) the observed 'rollover' in the effective attenuation coefficient. That is, instead of attenuation increasing monotonically with frequency, it reaches a maximum value before starting to drop again.

The operator D_t is the material derivative, or the time derivative in a reference frame moving with the wave (the Lagrangian reference frame) at the group velocity c_{g}. We can also reconfigure the above problem, in between breaking events, in the Lagrangian frame, as

$$\frac{\mathrm{d}x}{\mathrm{d}t} = c_{\text{g}}(\omega, x, t_*), \tag{4a}$$

$$\frac{\mathrm{d}}{\mathrm{d}x} S(\omega; x, t) = -\hat{\alpha}(\omega; x, t_*, S_*) S(\omega; x, t), \tag{4b}$$

where t_* is the last time ice breakage occurred at x, and $S_*(\omega, x) = S(\omega; x, t_*)$. Thus we have separated the problem into an advection problem and an attenuation one, and in our numerical scheme presented in Part 2, we solve (2) by alternately advecting and attenuating.

3.2. Ice breakage

We take a probabilistic approach to define a criterion for ice breakage. It is therefore helpful to revise some relationships between the SDF (S) and different wave statistics, before defining the breaking criterion itself.

3.2.1. Wave energy and statistics

We assume that the sea surface elevation, η, follows a Gaussian distribution, and neglect non-linear effects that cause slight asymmetry (Cartwright and Longuet-Higgins, 1956; Vaughan and Squire, 2011). The mean square sea surface elevation (vertical displacement from the mean water level), or the variance in the position of a water particle at the sea surface, $\langle \eta^2 \rangle = m_0[\eta]$, can be obtained from S via the formula

$$m_n[\eta] = \int_0^\infty \omega^n S(\omega) \mathrm{d}\omega, \tag{5}$$

(WMO, 1998). (We will also use the second spectral moment, m_2, later on.) The significant wave height is defined by $H_\mathrm{s} = 4\sqrt{m_0[\eta]}$.

Wave heights generally follow a Rayleigh distribution, for which the probability of a wave amplitude A exceeding a certain value A_c is approximately

$$\mathbb{P}(A > A_c) = \exp\left(-A_c^2/\langle A^2 \rangle\right), \tag{6}$$

(Longuet-Higgins, 1952, 1980), where $\langle A^2 \rangle$ denotes the mean square amplitude. If the wave spectrum has a narrow bandwidth and non-linear effects are negligible (low wave steepness), then $\langle A^2 \rangle = 2m_0[\eta]$, so

$$\mathbb{P}(A > A_c) = \exp\left(-A_c^2/2m_0[\eta]\right). \tag{7}$$

The mean square displacement of the ice is approximately $\langle \eta_\mathrm{ice}^2 \rangle = m_0[\eta_\mathrm{ice}]$, where

$$m_n[\eta_\mathrm{ice}] = \int_0^\infty \omega^n S(\omega) W^2(\omega) \mathrm{d}\omega. \tag{8}$$

Here $W(\omega) \approx k_\mathrm{ice}|\mathcal{T}|/k$, where $\mathcal{T}$ is the transmission coefficient for a wave traveling from water into ice (e.g. Williams and Porter, 2009), represents the amplitude response at each frequency of an ice floe to forcing from a wave of unit amplitude in the water surrounding it. The wave number $k(\omega) = \omega^2/g$ is the usual deep water propagating wave number, while $k_\mathrm{ice}(\omega)$ is the positive real root of (A.7), the dispersion relation for a section of ice-covered ocean.

The probability of A_ice exceeding a certain value A_c is

$$\mathbb{P}(A_\mathrm{ice} > A_\mathrm{c}) = \exp(-A_\mathrm{c}^2/2m_0[\eta_\mathrm{ice}]), \tag{9}$$

which is analogous to equation (7). In addition, we can also estimate the number of waves we expect in a given time interval Δt, N_W, as

$$N_\mathrm{W} = \frac{\Delta t}{2\pi}\sqrt{\frac{m_2[\eta_\mathrm{ice}]}{m_0[\eta_\mathrm{ice}]}}, \tag{10}$$

(WMO, 1998). (Note that factors in equations 7 and 10 have been corrected from their counterparts in Cartwright and Longuet-Higgins, 1956.) More precisely, this is the number of times we can expect a particle to cross its point of mean displacement in a downward direction. The quantity N_{W} also defines a representative wave period

$$T_{\mathrm{W}} = \frac{\Delta t}{N_{\mathrm{W}}} = 2\pi\sqrt{\frac{m_0[\eta_{\mathrm{ice}}]}{m_2[\eta_{\mathrm{ice}}]}}, \tag{11}$$

for the spectrum S at a given point and a representative (ice-coupled) wavelength of $\lambda_{\mathrm{W}} = 2\pi/k_{\mathrm{W}}$, where $k_{\mathrm{W}} = k_{\mathrm{ice}}(2\pi/T_\omega)$. The symbol T_{W} is sometimes written $T_{m_{0,2}}$ but we use the former to avoid clutter in our equations. Also note the factor of 2π is necessary since we define the moments m_n in terms of ω, rather than the frequency $1/T$.

We can also define analogous quantities for the strain, which for a thin elastic plate is defined as $\varepsilon = (h/2)\partial_x^2\eta_{\mathrm{ice}}$. Therefore, its mean square value is $\langle\varepsilon^2\rangle = m_0[\varepsilon]$, where

$$m_n[\varepsilon] = \int_0^\infty \omega^n S(\omega)E^2(\omega)\mathrm{d}\omega, \quad E(\omega) = \frac{h}{2}k_{\mathrm{ice}}^2 W(\omega). \tag{12}$$

The latter is the approximate strain amplitude per metre of water displacement amplitude for a monochromatic wave of the form $\eta_{\mathrm{ice}} = A_{\mathrm{ice}}\cos(k_{\mathrm{ice}}x - \omega t)$ (with $A = 1\,\mathrm{m}$, so $A_{\mathrm{ice}} = W\,\mathrm{m}$). It does not account for non-linear interactions between frequencies, which could potentially be important approaching an ice breakage event. For now we assume brittle failure of the ice, so that a linear stress-strain law applies right up to the point where the ice breaks. If we now define the significant strain amplitude to be $E_{\mathrm{s}} = 2\sqrt{m_0[\varepsilon]}$, which is two standard deviations in strain, then the probability of the maximum strain from a passing wave E_{W} exceeding a breaking strain ε_c is

$$\mathbb{P}_\varepsilon = \mathbb{P}(E_{\mathrm{W}} > \varepsilon_{\mathrm{c}}) = \exp(-\varepsilon_{\mathrm{c}}^2/2m_0[\varepsilon]) = \exp(-2\varepsilon_{\mathrm{c}}^2/E_{\mathrm{s}}^2). \tag{13}$$

3.2.2. Breaking criterion

To determine whether the ice will be broken by waves, we define a critical probability threshold $\mathbb{P}_{\mathrm{c}}$ such that if $\mathbb{P}_\varepsilon > \mathbb{P}_{\mathrm{c}}$ the ice will break. If it breaks, the maximum floe size is set to $D_{\max} = \max(\lambda_{\mathrm{W}}/2, D_{\min})$ where $D_{\min}$ is the size below which waves are not significantly attenuated and is set to 20m (Kohout, 2008). These two quantities $D_{\min}$ and $D_{\max}$ determine the FSD (see §4.1).

From (13), the criterion $\mathbb{P}_\varepsilon > \mathbb{P}_\mathrm{c}$ can be written in terms of E_s, ε_c and $\mathbb{P}_\mathrm{c}$ as

$$E_\mathrm{s} > E_\mathrm{c} = \varepsilon_\mathrm{c}\sqrt{-2/\log\left(\mathbb{P}_\mathrm{c}\right)}. \tag{14}$$

Thus the single parameter E_c combines the effects of both ε_c and $\mathbb{P}_\mathrm{c}$. Note that $\mathbb{P}_\mathrm{c} = \mathrm{e}^{-2} \approx 0.14$ corresponds to the criterion of Langhorne et al. (2001), i.e. $E_\mathrm{s} > \varepsilon_\mathrm{c}$, and the upper limit tested by Vaughan and Squire (2011).

The default value for $\mathbb{P}_c$ that will be used in our numerical results is based on the condition for a narrow spectrum. For a monochromatic wave that produces a strain amplitude E_W, the breaking condition would be $E_\mathrm{W} > \varepsilon_\mathrm{c}$. Therefore, since $\langle\varepsilon^2\rangle = E_\mathrm{W}^2/2$ in that case, the breaking condition is $E_\mathrm{s} > \varepsilon_\mathrm{c}\sqrt{2}$. This corresponds to choosing $\mathbb{P}_\mathrm{c} = \mathrm{e}^{-1} \approx 0.37$ in (14). We note that this value is easily changed in our model when better observational information becomes available.

4. Model sub-components

4.1. Floe size distribution

Prior to 2006, numerous researchers (e.g. Weeks et al., 1980; Rothrock and Thorndike, 1984; Matsushita, 1985; Holt and Martin, 2001; Toyota and Enomoto, 2002) made observations of floe sizes in Arctic areas. It was found that the FSD generally obeyed a power-law (Pareto) distribution, where the probability of finding a floe diameter D greater than D_* is given by

$$\mathbb{P}(D > D_*) = P(D) = (D_\mathrm{min}/D_*)^\gamma \quad \text{for } D > D_\mathrm{min}, \tag{15}$$

where D_min is the minimum floe diameter. The expected value of D^n is therefore

$$\left\langle D^n\right\rangle = -\int_{D_\mathrm{min}}^{\infty} D^n\partial_D P(D)\mathrm{d}D = \frac{\gamma}{\gamma-n}D_\mathrm{min}^n.$$

The fitted exponent γ was usually found to be greater than 2, which implies that the expected diameter and area are defined. However, there are problems with trying to treat small floes with the above distribution, i.e. if we try to let $D_\mathrm{min} \to 0$. Therefore Toyota et al. (2006) investigated the FSD of small floes of diameter 1 m–1.5 km, using data obtained from the southern Sea of Okhotsk. They found that floes smaller than about 40 m still obeyed a power law, but were best fitted by a smaller value of γ (about 1.15). This regime shift was also observed in Antarctica in the late winter of 2006 and 2007 by Toyota et al. (2011), based on observations in the northwestern Weddell Sea and off Wilkes Land (around 64°S, 117°E) with a helicopter-borne digital video camera. Concurrent ice thickness measurements were also made, using a helicopter-borne electromagnetic (EM) sensor above the Weddell Sea and a video system off Wilkes land. The regime shift was consistent with the value

$$D_{\mathrm{c}} = \left(\frac{\pi^4 Y h^3}{48\rho g(1-\nu^2)} \right)^{1/4}, \tag{16}$$

which corresponds to the diameter below which flexural failure cannot occur (Mellor, 1986).

Toyota et al. (2011) proposed an explanation of the exponent governing the smaller floes in terms of a breaking probability Π, related to γ by

$$\Pi = \xi^{\gamma-2} \quad \text{or} \quad \gamma = 2 + \log_\xi \Pi, \tag{17}$$

where Π is the probability that a floe will break into ξ^2 pieces. A similar explanation was suggested by Herman (2010), who proposed a generalised Lotka-Volterra model for the implementation of breaking. Such models produce distributions that are asymptotically like power-law distributions, but with better behaviour near $D = 0$ (i.e. D_{min} can be zero).

Note that the model of Toyota et al. (2011) always predicts $\gamma < 2$, so other mechanisms are required to explain the exponent for the larger floes being greater than 2. Toyota et al. suggested herding with subsequent freezing together of floes could be one explanation. The simulations of Herman (2011) lent credibility to this as they showed that floes tended to group together in clusters, and that the diameter of these clusters obeyed power-law distributions with exponents often greater than 2 (depending on the concentration).

We use the simpler approach of DKB, who restricted themselves to small floes and took the FSD to be over the finite interval of $D_{\mathrm{min}} < D < D_{\mathrm{max}}$. The distribution inside was based on the ideas and parameters of Toyota et al. (2011), deriving a novel formula for the mean floe size $\langle D \rangle$. We set (as they did), the fixed values of $D_{\mathrm{min}} = 20\,\mathrm{m}$, $\xi = 2$, and $\Pi = 0.9$. It is important that D_{min} is not too small as $\hat{\alpha}$, as given by (3), will be very large when $\langle D \rangle$ is small. However, Kohout and Meylan (2008) found that floes with lengths less than 20 m produced negligible scattering, so this value of D_{min} is a reasonable choice. It may also be possible to relate Π to our breaking probabilities in the future.

4.2. Attenuation models

As discussed in §1, attenuation models based on multiple wave scattering are closely linked to the FSD since waves encounter more floe edges after ice breakage occurs, and hence more scattering events occur. Viscosity models only depend on the concentration and are unaffected by ice breakage. We implement an attenuation model in which wave scattering is the dominant attenuation mechanism, but we also include additional attenuation provided by a particular damping model due to Robinson and Palmer (1990). Accordingly, the dimensional and non-dimensional attenuation coefficients are written, respectively,

$$\alpha = \alpha^{\text{scat}} + \alpha^{\text{visc}} \quad \text{and} \quad \hat{\alpha} = \hat{\alpha}^{\text{scat}} + \hat{\alpha}^{\text{visc}}. \tag{18}$$

4.2.1. Multiple wave scattering attenuation models

The multiple scattering model is based on linear wave theory. The model predicts the spatial profile of time-harmonic waves in a fluid domain, which has a surface that is partially covered by a large number of floes. The floes are represented by thin-elastic plates and respond to fluid motion in flexure only. The wave number for the ice-covered ocean is k_{ice} and for the open ocean is k. In general $k_{\text{ice}} \neq k$, so scattering is produced by an impedance change when a wave moves from the open ocean into a patch of ice-covered ocean, or vice versa, at a floe edge.

Attenuation due to multiple wave scattering by floe edges alone is sufficient for the present investigation (Bennetts and Squire, 2012b), but extensions to scattering by other features in the ice cover, e.g. cracks and pressure ridges, are possible (see Bennetts and Squire, 2012a).

The model is confined to two-dimensional transects, i.e. one horizontal dimension and one depth dimension (see Appendix A). It cannot yet account for lateral energy leakage or directional evolution of the waves. Attenuation models capable of describing these features are being developed (Bennetts et al., 2010), but are not yet sufficiently robust to be integrated into the WIM. Even with the restriction to only one horizontal dimension, computational expense can be large as there is an infinite sum of reflections and transmissions of the wave between each pair of adjacent floe edges. In the full multiple scattering problem exponential decay is a product of localization theory, which relies on positional disorder and requires proper consideration of wave phases.

Reliance on disorder implies the use of an averaging approach. The attenuation coefficient due to multiple wave scattering is hence calculated as an ensemble average of the attenuation rates produced in simulations that are randomly selected from prescribed distributions. It is natural to calculate a non-dimensional attenuation coefficient, α^{scat} (i.e. per floe), for these types of problem, but this is easily mapped onto the dimensional attenuation coefficient $\hat{\alpha}^{\mathrm{scat}}$ (i.e. per meter) for use in the WIM. The distribution of floes used in the model has a large impact on the predicted attenuation and hence the width of the MIZ. This will be demonstrated using numerical results below, and the underlying reasons will discussed at that point.

4.2.2. Viscosity-based attenuation models

Recent model-data comparisons (Perrie and Hu, 1996; Kohout and Meylan, 2008; Bennetts et al., 2010) have shown that multiple wave scattering models give good agreement with data for mid-range periods (6–15 s quoted by Kohout and Meylan, 2008). For large periods, however, scattering is negligible and other unmodeled dissipative mechanisms are more important, although it is unclear which mechanism is dominant in this regime. Plausible candidates include secondary creep occurring when flexural strain rates are slower, and frictional dissipation at the ice-water interface. While this issue remains unresolved, the attenuation of large period waves is modeled here with the damped thin elastic plate model of Robinson and Palmer (1990) (see Appendix A). It contains a single damping coefficient Γ, which produces a drag force that damps particle oscillations at the ice-water interface.

In practice, we solve the dispersion relation (A.7) and use the imaginary part of the damped-propagating wavenumber $\mathcal{K}(\omega,\Gamma) \approx k_{\mathrm{ice}} + \mathrm{i}\delta$ (see Appendix A), and set the viscous attenuation coefficients to be

$$\alpha^{\mathrm{visc}} = 2\delta\langle D\rangle \quad \text{and} \quad \hat{\alpha}^{\mathrm{visc}} = 2\delta c. \tag{19}$$

The magnitude of the damping coefficient, Γ, is set using data from the most complete single experiment on wave attenuation available at present, that of Squire and Moore (1980). More experimental data, with detailed descriptions of prevailing ice properties and wave conditions, would help to tune Γ or to compare different models of wave dissipation.

Most other viscosity-based attenuation models take a similar but more complicated approach and model the ice as being an incompressible viscous fluid or viscoelastic medium of finite thickness, with constitutive relations involving tuned viscosity parameters. The attenuation rate from these models is also typically predicted by solving a dispersion relation and finding the analogous parameter to δ.

Weber (1987) assumed that the ice was so viscous that it was in quasi-static equilibrium, with pressure and friction balancing each other out. The ocean was also given a viscosity which was tuned to roughly agree with observations. De Carolis and Desiderio (2002) developed this model further by letting the ice viscosity take a finite value. Wang and Shen (2011b) used a viscoelastic model for the sea ice, but with the underlying ocean taken to be inviscid.

An associated model in which attenuation is produced by drag due to the bottom roughness of floes was proposed by Kohout et al. (2011). This also has a drag coefficient which requires tuning. However, it is notable that the model of Kohout et al. (2011) does not predict exponential attenuation.

4.2.3. Comparison of two attenuation models

Figure B.2 shows comparisons of predictions made by two different versions of the attenuation model. The first model considered, denoted A and constructed for this paper only, uses a seemingly plausible choice for the distributions. The FSD is based on a power law discussed in §4.1, which was observed for small floes ($\lesssim$ 20–40 m) in Antarctic locations (Toyota et al., 2011). Floe separations are arbitrarily generated from an exponential distribution $\mathbb{P}(G > g) = \exp(-g/\langle G\rangle)$, with $\langle G\rangle = \langle D\rangle(c^{-1} - 1)$ and in this example the ice concentration is $c = 0.9$, although the discussion applies equally well to any concentration. The attenuation coefficient $\alpha = \alpha^{\mathrm{scat}}$ ($\alpha^{\mathrm{visc}} = 0$ for this model) is calculated as the average of 100 randomly generated simulations.

The second model, denoted B, is based on the recent work of Bennetts and Squire (2012b). Rather than considering spatial distributions, Bennetts and Squire considered the wave phases as uniformly-distributed random variables and averaged over all possibilities. They argued that the model is not intended as a true replica of the MIZ, so detailed predictions about the exact distribution of wave phases cannot be relied upon. An assumption of uniformity is thus the simplest possible in the absence of a more realistic model. In this setting the attenuation coefficient may be calculated analytically rather than relying on a numerical approximation. The expression for the attenuation coefficient can be simplified further if the floes are assumed to be long, so that only the reflection produced by a single floe edge is required, and the attenuation coefficient due to scattering is then given by $\alpha^{\mathrm{scat}} = -2\log(1 - |\mathcal{R}|^2)$, where $\mathcal{R}$ is the reflection coefficient by the edge of a semi-infinite floe of the specified thickness (calculated here using the method of Williams and Porter, 2009). Model B is also adapted to include the effect of viscous scattering (for different values of Γ), i.e.

$$\alpha \equiv \alpha^{\mathrm{scat}} + \alpha^{\mathrm{visc}} = -2\log(1 - |\mathcal{R}|^2) + 2\delta\langle D\rangle. \tag{20}$$

Figures B.2(a, b) show the attenuation coefficients produced by the different attenuation models, computed for two different ice thicknesses, and different values of the viscosity parameter (model B only). Because the B curves with $\Gamma = 13\,\mathrm{Pa\,s\,m^{-1}}$ include an empirical inelastic contribution, they produce the greatest attenuation for large periods. As expected from Appendix A, the damping is also less pronounced as the thickness increases. The value $\Gamma = 13\,\mathrm{Pa\,s\,m^{-1}}$ was fitted using the attenuation coefficients for the three largest periods of Squire and Moore (1980) (see Table 2). They were measured for thinner ($h \sim 0.5\,\mathrm{m}$) Bering Sea ice, so we used $h = 0.5\,\mathrm{m}$ in our tuning procedure.

Curves corresponding to model A are markedly different from the other curves. Due to the small values of average floe length $\langle D\rangle$ (in Figure B.2a, $\langle D\rangle$ is approximately $40\,\mathrm{m}$, while in Figures B.2b-d it is about $64\,\mathrm{m}$), the attenuation of large period waves is several orders of magnitude too small, which qualitatively contradicts the observations of Squire and Moore (1980) mentioned above. There is also some additional fine structure in the attenuation from model A for lower periods. In particular, there is an interval of periods between about $6\,\mathrm{s}$ and $12\,\mathrm{s}$ (the interval moves to higher periods as ice thickness increases), where there is much less attenuation than the other models. This has a profound effect on the ice breakage that is able to be produced by model A, as waves from that range of periods can produce very large strains if they remain unattenuated.

In Figures B.2(c-d), we show the effects of the different attenuation models on the signficant wave height H_{s} and the significant strain E_{s} as they travel into an ice field. As a simple example spectrum, we take the initial wave spectrum, S_0, to be a Bretschneider spectrum, i.e.

$$S_0(\omega) = \frac{1.25H_{\mathrm{s}}^2T^5}{8\pi T_{\mathrm{p}}^4}\mathrm{e}^{-1.25(T/T_{\mathrm{p}})^4}, \tag{21}$$

where $T = 2\pi/\omega$ is the period, T_{p} is the peak period ($7\,\mathrm{s}$ in this example). Initially $H_{\mathrm{s}} = 1\,\mathrm{m}$, but in general, after traveling past N floes it and E_{s} are given by

$$H_{\mathrm{s}} = 4\sqrt{m_0^{(N)}[\eta_{\mathrm{ice}}]}, \quad E_{\mathrm{s}} = 2\sqrt{m_0^{(N)}[\varepsilon]}, \tag{22}$$

where

$$m_0^{(N)}[\eta_{\rm ice}] = \int S_0(\omega) W^2(\omega) \mathrm{e}^{-\alpha(\omega)N} \mathrm{d}\omega, \tag{23a}$$

$$m_0^{(N)}[\varepsilon] = \int S_0(\omega) E^2(\omega) \mathrm{e}^{-\alpha(\omega)N} \mathrm{d}\omega. \tag{23b}$$

The significant effect of the FSD on the attenuation model is further illustrated in Figures B.2(c-d), which show how both the signficant wave height $H_{\rm s}$ and the significant strain $E_{\rm s}$ decay with N, the number of floes that the waves have passed. After only a small number of floes it can be seen that $H_{\rm s}$ and $E_{\rm s}$ for model A (chained curve) are several orders of magnitude larger than for the other two curves, which are roughly the same.

We can also see that for model A, $E_{\rm s}$ remains very close to the approximate breaking strain for the range of values of N that are plotted. Both $E_{\rm s}$ curves produced by model B drop below $E_{\rm c}$ after a relatively small number of floes. This suggests that the width of the MIZ, $L_{\rm MIZ}$, will be similarly small under either of these models but will be significantly larger for model A if strain failure is the main breakage mechanism. In fact, in simulations involving model A (not presented), we found that a 450-km transect was almost always entirely broken, when the expected range is about 50–200 km. We therefore disregard model A for the numerical results presented in Part 2, on the basis that the predicted attenuation rates are insufficient to replicate what is observed. Note that the power-law FSD model is still used for the WIM itself.

4.3. Ice properties

Timco and O'Brien (1994) collate and analyse nearly a thousand flexural strength measurements conducted by 14 different investigators under a variety of conditions and test types, namely, *in situ* cantilever tests and simple beam tests with 3- or 4-point loading, to show that the flexural strength $\sigma_{\rm c}$ has the following very simple dependence on brine volume fraction $\upsilon_{\rm b}$:

$$\sigma_{\rm c} = \sigma_0 \exp\left(-5.88\sqrt{\upsilon_{\rm b}}\right), \tag{24}$$

where $\sigma_0 = 1.76$ MPa. This is plotted in Figure B.3(a), and shows a monotonic decrease from σ_0 as $\upsilon_{\rm b}$ increases. Brine volume is often a parameter in ice-ocean models but, if necessary, it can also be calculated from the ice temperature and salinity, using the formula of Frankenstein and Gardner (1967).

Flexural strength tests are normally analyzed by means of Euler-Bernoulli beam theory, in which the stress normal to the beam cross section is related to the analogous strain. In principle, therefore, to convert flexural strength into a breaking strain ε_c for a beam of sea ice, all we require is the Young's modulus Y for sea ice.

In the course of a typical flexural strength test and during the recurring cyclic flexure imparted by ocean surface gravity waves, it is expected that the sea ice will experience stress levels and rates such that the total recoverable strain $\varepsilon^\mathrm{T} \approx \varepsilon^\mathrm{i} + \varepsilon^\mathrm{d}$, where ε^i is the instantaneous elastic strain and ε^d is the delayed elastic (i.e. anelastic) strain, also known as primary, recoverable creep. This suggests a variation on the instantaneous elastic Young's modulus Y which allows for delayed elasticity to act, which is often called the effective modulus or the strain modulus and that we shall denote by Y^*.

Timco and Weeks (2010) report a linear relationship for $Y(\upsilon_\mathrm{b})$ of the form $Y = Y_0(1-3.51\upsilon_\mathrm{b})$, where $Y_0 \approx 10\,\mathrm{GPa}$ is roughly the value for freshwater ice at high loading rates. But, whilst increased brine volume leads to a reduction in the effective modulus Y^*, the data are too scattered for an empirical relationship for $Y^*(\upsilon_\mathrm{b})$ to be expressed. For "average" brine volumes ranging from 50 to 100 ppt ($\upsilon_\mathrm{b} = 0.05$ to 0.1, Frankenstein and Gardner, 1967), this suggests Y will reduce to between $\sim$ 6–8 GPa.

As we have noted above, the effect of brine volume on Y^* is more difficult to pin down, but we believe the same kind of reduction would not be unreasonable. More challenging is determining the effect of anelasticity (delayed elasticity) on reducing Y to Y^*. The mechanisms that achieve this power-law primary creep with no microcracking cause relaxation processes to occur during cyclical loading, so the rate of loading is important. Few data can help us here but Figure 4 of Cole (1998) shows model predictions for the effective modulus at four loading frequencies that include those associated with surface gravity wave periods, i.e. 10^{-2}–10^{0} Hz (or 0.01–1 Hz), and, incidentally, the reduction in Y due to total porosity, i.e. air plus brine. The latter effects are comparable in magnitude to the reductions in Y given above; the effect of rate is about 0.5 GPa as wave period is changed from 1 s to 10 s, and about 1 GPa from 10 s to 100 s. We therefore consider a reduction of 1 GPa is reasonable in our model, and in summary we use

$$Y^* = Y_0(1 - 3.51\upsilon_\mathrm{b}) - 1\mathrm{GPa}, \tag{25a}$$

$$\varepsilon_\mathrm{c} = \frac{\sigma_\mathrm{c}}{Y^*}. \tag{25b}$$

The effective Young's modulus and breaking strain given by equation (25) are plotted as functions of brine volume fraction in Figure B.3(b, c).

We observe that an appropriate choice of a value for the effective Young's modulus is important from the wave modeling perspective, as the higher Y^* becomes the more energy is reflected at each floe present and the greater the attenuation experienced by the wave train. However, because the same value of Y^* is used to convert from flexural stress to failure strain, the analysis is self-consistent.

The breaking strain has a minimum value of approximately 4.8×10^{-5} when $\upsilon_\mathrm{b} = 0.15$ ($Y^* = 3.8\,\mathrm{GPa}$). The value is approximately constant for $\upsilon_\mathrm{b} \in [0.1, 0.2]$. It shows an increase for both higher and lower brine volumes — the less porous ice is predictably stronger, while the more porous ice is more compliant so will be able to sustain more bending before breaking. If $\upsilon_\mathrm{b} = 0.05$, $\varepsilon_\mathrm{c} \approx 6.5 \times 10^{-5}$ ($Y^* = 7.2\,\mathrm{GPa}$), while if $\upsilon_\mathrm{b} = 0.1$, the breaking strain drops to $\varepsilon_\mathrm{c} \approx 5.0 \times 10^{-5}$ ($Y^* = 5.5\,\mathrm{GPa}$). Although lower values of Y^* have been measured in the field, (e.g. by Marchenko et al., 2011, in the Svalbard fjords), the temporal and spatial variability of sea ice, and the origin and special character of the ice floes in the East Greenland Current, suggests it is wiser to use the value for Y^* we have deduced, noting that it is a straightforward matter to change it.

The final property we will need to consider in our wave modeling is Poisson's ratio. Langleben and Pounder (1963) determined it to be $\nu = 0.295 \pm 0.009$ from seismic measurements, so in most wave calculations involving ice (e.g. Fox and Squire, 1991) it is simply taken to be 0.3.

5. Summary and discussion

We have set the theoretical foundations of a waves-in-ice model (WIM) in this, Part 1 of a two-part series. The WIM will provide the first link between wave models, e.g. WAM, WAVEWATCH III, and sea ice models, e.g. CICE, LIM. The primary output of the WIM is a floe size distribution (FSD), which can be used to define the marginal ice zone (MIZ) as a subregion of the ice mask. The FSD will then be available as an input for MIZ-specific dynamic and thermodynamic models in future research.

Wave-ice interactions occurring in an MIZ comprise

(i) the attenuation of the waves due to the presence of ice cover; and

(ii) the breaking of the ice cover due to wave motion.

The WIM proposed in this work includes both components. It is a more developed version of the WIM proposed by Dumont et al. (2011), which, to our knowledge, was the first published model to combine attenuation and ice breakage.

We advect the wave spectrum, S, through the ice-covered ocean using a modified version of the energy balance equation. We neglected parameterizations of dissipation due to all conventional sources, e.g. winds and white-capping, and also non-linear interactions. However, we included a new term, $R_{\rm ice} = \hat{\alpha}S$, which parameterizes dissipation due to the ice cover.

We used an attenuation model to calculate the attenuation coefficient, $\hat{\alpha}$, which defines the rate of exponential decay of the waves. The multiple wave scattering, attenuation model of Bennetts and Squire (2012b) was summarized. We noted striking differences in the attenuation coefficient when using a seemingly plausible power-law FSD in the attenuation model, rather than the random wave phase model proposed by Bennetts and Squire (2012b). Furthermore, we included viscous damping to simulate the unmodeled attenuation of large period waves.

We considered the attenuation coefficient to be a function of wave frequency and also to depend on the properties of the ice cover, including the FSD. The power-law FSD model of Toyota et al. (2011) was used for local regions of the ice cover in the WIM. We created a link between the FSD model and the local wave spectrum by setting the maximum floe size to be half the dominant wavelength if the wave spectrum was sufficient to cause the ice to break. Breakage would therefore abruply alter the FSD, and consequently the attenuation coefficient, in the WIM.

We outlined a criterion to determine the occurrence of ice breakage. The criterion was based on the integrated strains imposed on the ice by the passing wave spectrum. We derived a critical strain, which incorporates a critical probability and a breaking strain, above which ice breakage was applied. In the absence of experimental or theoretical data, the value of the critical probability was set according to the limit for monochromatic waves.

The mechanical properties of the ice cover provide important input parameters for the attenuation model and the ice breakage criterion. We formulated an expression for the breaking strain, by means of a relationship for flexural strength due to Timco and O'Brien (1994) using an Euler-Bernoulli beam model for the sea ice. Further, we also proposed the use of an effective Young's modulus in this relationship, so that both instantaneous and delayed elasticity are incorporated, and derived an expression for this quantity.

The above summary highlights the presence of uncertainties in the model. These are: (i) the viscosity parameter that determines the attenuation of large period waves; (ii) the breaking strain of the ice cover; and (iii) the critical probability above which the ice will break. Sensitivity studies are therefore required with respect to these quantities, and this forms the kernel of the numerical study that follows in Part 2. An additional uncertainty in the model is the amount of wave energy lost during ice breakage. Our treatment of the energy loss is closely related to the numerical implementation of the WIM, and its discussion is therefore contained entirely in Part 2.

The numerical implementation of the WIM itself is non-trivial and a full description of our methods are given in Part 2.

Acknowledgement

The work described herein is embedded within the Waves-in-Ice Forecasting for Arctic Operators (WIFAR) project, coordinated by Nansen Environmental and Remote Sensing Center (NERSC) and funded by the Research Council of Norway and Total E&P Norge through the Programme for Optimal Management of Petroleum Resources (PETROMAKS). The authors acknowledge with gratitude this funding and the support of the University of Otago, New Zealand. They thank Aleksey Marchenko for useful discussions, and also thank the anonymous reviewers of this and earlier revisions of this paper for their constructive criticisms.

References

Ardhuin, F., Rascle, N., Belibassakis, K. A., 2008. Explicit wave-averaged primitive equations using a generalized Lagrangian mean. Ocean Modelling 20 (1), 35–60.

Ardhuin, F., Rogers, E., Babanin, A. V., Filipot, J.-F. Magne, R., Roland, A., van der Westhuysen, A., Queffeulou, P., Lefevre, J.-M., Aouf, L., Collard, F., 2010. Semiempirical dissipation source functions for ocean waves. Part I: Definition, calibration, and validation. J. Phys. Oceanogr. 40, 1917–1941.

Asplin, M. G., Galley, R., Barber, D. G., Prinsenberg, S. J., 2012. Fracture of summer perennial sea ice by ocean swell as a result of Arctic storms. J. Geophys. Res. 117 (C06025).

Babanin, A. V., Ganopolski, A., Phillips, W. R. C., 2009. Wave-induced upper-ocean mixing and climate modelling. Ocean Modelling 29 (3), 189–197.

Barber, D. G., Galley, R., Asplin, M. G., De Abreu, R., Warner, K.-A., Pućko, M., Gupta, M., Prinsenberg, S. J., Julien, S., 2009. Perennial pack ice in the southern Beaufort Sea was not as it appeared in the summer of 2009. Geophys. Res. Lett. 36 (L24501).

Bennetts, L., Peter, M. A., Squire, V. A., Meylan, M. H., 2010. A three-dimensional model of wave attenuation in the marginal ice zone. J. Geophys. Res. 115 (C12043).

Bennetts, L. G., Squire, V. A., 2012a. Model sensitivity analysis of scattering-induced attenuation of ice-coupled waves. Ocean Modelling 45–46, 1–13.

Bennetts, L. G., Squire, V. A., 2012b. On the calculation of an attenuation coefficient for transects of ice-covered ocean. Proc. R. Soc. Lond. A 468 (2137), 136–162.

Cartwright, D. E., Longuet-Higgins, M. S., 1956. The statistical distribution of the maxima of a random function. Proc. R. Soc. Lond. A 237 (1209), 212–232.

Cole, D. M., 1998. Modeling the cyclic loading response of sea ice. Int. J. Solids Struct. 35 (31—32), 4067—4075.

De Carolis, G., Desiderio, D., 2002. Dispersion and attenuation of gravity waves in ice: a two-layer viscous fluid model with experimental data validation. Physics Letters A 305, 399–412.

Doble, M. J., Bidlot, J.-R., submitted. Wavebuoy measurements at the Antarctic sea ice edge compared with an enhanced ECMWF WAM: progress towards global waves-in-ice modeling. Ocean Modelling.

Dumont, D., Kohout, A. L., Bertino, L., 2011. A wave-based model for the marginal ice zone including a floe breaking parameterization. J. Geophys. Res. 116 (C4), 1–12.

Feltham, D. L., 2005. Granular flow in the marginal ice zone. Phil. Trans. R. Soc. Lond. A. 363, 1677–1700.

Fox, C., Squire, V. A., 1991. Strain in shore fast ice due to incoming ocean waves and swell. J. Geophys. Res. 96 (C3), 4531–4547.

Frankenstein, G. E., Gardner, S., 1967. Equations for determining the brine volume of sea ice from -0.5 to 22.9°C. J. Glaciol. 6, 943—944.

Gelci, R., Cazalé, H., Vassal, J., 1957. Prévision de la houle. La méthode des densités spectroangulaires. Bull. Infor. Comité Central Oceanogr. d'Etude Côtes 9, 416–435.

Girard, L., Amitrano, D., Weiss, J., 2010. Failure as a critical phenomenon in a progressive damage model. Journal of Statistical Mechanics: Theory and Experiment P01013.

Girard, L., Weiss, J., Molines, J. M., Barnier, B., Bouillon, S., 2009. Evaluation of high-resolution sea ice models on the basis of statistical and scaling properties of Arctic sea ice drift and deformation. J. Geophys. Res. 114 (C08015).

Hasselmann, K., 1960. Grundgleichungen der seegangsvoraussage. Schiffstechnik 7, 191–195.

Hasselmann, K., 1962. On the non-linear transfer in a gravity-wave spectrum. Part 1. General Theory. J. Fluid Mech. 12, 481–500.

Hasselmann, K., 1963. On the non-linear transfer in a gravity-wave spectrum. Part 3. Computation of the energy flux and swell-sea interaction for a Neumann spectrum. J. Fluid Mech. 15, 385–398.

Herman, A., 2010. Sea-ice floe-size distribution in the context of spontaneous scaling emergence in stochastic systems. Phys. Rev. E 81, 066123.

Herman, A., 2011. Molecular-dynamics simulation of clustering processes in sea-ice floes. Phys. Rev. E 84, 056104.

Herman, A., 2013. Numerical modeling of force and contact networks in fragmented sea ice. Ann. Glaciol. 54 (62), 114–120.

Hibler, W. D., 1979. A dynamic thermodynamic sea ice model. J. Phys. Oceanogr. 9, 815–846.

Holt, B., Martin, S., 2001. The effect of a storm on the 1992 summer sea ice cover of the Beaufort, Chukchi, and East Siberian Seas. J. Geophys. Res. 106 (C1), 1017–1032.

Howells, 1960. The multiple scattering of waves by weak random irregularities in the medium. Proc. R. Soc. A 252, 431–462.

Hunke, E. C., Dukowicz, J. K., 1997. An elastic–viscous–plastic model for sea ice dynamics. J. Phys. Oceanogr. 27, 1849–1867.

Keller, J. B., 1998. Gravity waves on ice-covered water. J. Geophys. Res. 103 (C4), 7663–7670.

Kohout, A., Meylan, M., Plew, D. R., 2011. Wave attenuation in a marginal ice zone due to the bottom roughness of ice floes. Ann. Glaciol. 52 (57), 118–122.

Kohout, A. L., Meylan, M. H., 2008. An elastic plate model for wave attenuation and ice floe breaking in the marginal ice zone. J. Geophys. Res. 113 (C09016), doi:10.1029/2007JC004434.

Langhorne, P. J., Squire, V. A., Fox, C., Haskell, T. G., 1998. Break-up of sea ice by ocean waves. Annals of Glaciology 27, 438–442.

Langhorne, P. J., Squire, V. A., Fox, C., Haskell, T. G., 2001. Lifetime estimation for a land-fast ice sheet subjected to ocean swell. Annals of Glaciology 33, 333–338.

Langleben, M. P., Pounder, E. R., 1963. Elastic parameters of sea ice. In: Kingery, W. D. (Ed.), Ice and snow. MIT Press, USA, pp. 69–78.

Longuet-Higgins, M. S., 1952. On the statistical distribution of the heights of sea waves. Journal of Marine Research 11, 245–266.

Longuet-Higgins, M. S., 1980. On the distribution of the heights of sea waves: Some effects of nonlinearity and finite band width. J. Geophys. Res. 85 (C3), 1519–1523.

Marchenko, A. V., Shestov, A., Karulin, E., Morozov, E., Karulina, M., Bogorodsky, P., Muzylev, S. V., Onishchenko, D., Makshtas, A., 2011. Field studies of sea water and ice properties in Svalbard fjords. In: Proceedings of the 21st International Conference on Port and Ocean Engineering under Arctic Conditions. Montréal, Canada, pp. 148–160.

Masson, D., LeBlond, P. H., 1989. Spectral evolution of wind-generated surface gravity waves in a dispersed ice field. J. Fluid Mech. 202, 111–136.

Matsushita, M., 1985. Fractal viewpoint of fracture and accretion. Journal of the physical society of Japan 54 (3), 857–860.

Mellor, M., 1986. The mechanics of sea ice. In: Untersteiner, N. (Ed.), The Geophysics of Sea Ice. pp. 165–182.

Meylan, M., Squire, V., Fox, C., 1997. Toward realism in modelling ocean wave behaviour in marginal ice zones. Journal of Geophysical Research—Oceans 102 (C10), 22981–22991.

Meylan, M. H., Masson, D., 2006. A linear Boltzmann equation to model wave scattering in the marginal ice zone. Ocean Modelling 11 (3-4), 417–427.

Perrie, W., Hu, Y., 1996. Air–ice–ocean momentum exchange. Part 1: Energy transfer between waves and ice floes. J. of Phys. Ocean. 26, 1705–1720.

Polnikov, V., Lavrenov, I., 2007. Calculation of the nonlinear energy transfer through the wave spectrum at the sea surface covered with broken ice. Oceanology 47, 334–343.

Prinsenberg, S. J., Peterson, I. K., 2011. Observing regional-scale pack-ice decay processes with helicopter-borne sensors and moored upward-looking sonars. Ann. Glaciol. 52 (57), 35–42.

Rampal, P., Weiss, J., Marsan, D., Lindsay, R., Stern, H., 2008. Scaling properties of sea ice deformation from buoy dispersion analysis. J. Geophys. Res. 113 (C03002).

Robinson, N. J., Palmer, S. C., 1990. A modal analysis of a rectangular plate floating on an incompressible fluid. J. Sound Vib. 142, 453–460.

Rothrock, D. A., Thorndike, A. S., 1984. Measuring the sea ice floe size distribution. J. Geophys. Res. 89 (C4), 6477–6486.

Shen, H. H., Hibler, W. D., Leppäranta, M., 1986. On applying granular flow theory to a deforming broken ice field. Acta Mechanica 63, 143–160.

Shen, H. H., Sankaran, B., 2004. Internal length and time scales in a simple shear granular flow. Phys. Rev. E 70 (051308).

Squire, V., Moore, S. C., 1980. Direct measurement of the attenuation of ocean waves by pack ice. Nature 283 (5745), 365–368.

Steele, M., 1992. Sea ice melting and floe geometry in a simple ice-ocean model. J. Geophys. Res. 97 (C11), 17,729–17,738.

Steele, M., Morison, J. H., Untersteiner, N., 1989. The partition of air-ice-ocean momentum exchange as a function of ice concentration, floe size, and draft. J. Geophys. Res. 94 (C9), 12,739–12,750.

Stephenson, S. R., Smith, L. C., Agnew, J. A., 2011. Divergent long-term trajectories of human access to the Arctic. Nature Climate Change 1, 156–160.

Timco, G. W., O'Brien, S., 1994. Flexural strength equation for sea ice. Cold Regions Sci. Tech. 22, 285–298.

Timco, G. W., Weeks, W. F., 2010. A review of the engineering properties of sea ice. Cold Regions Sci. Tech. 60, 107–129.

Toyota, T., Enomoto, H., 2002. Analysis of sea ice floes in the Sea of Okhotsk using ADEOS/AVNIR images. In: Proc. 16th Int. Symposium on Ice, International Association for Hydro-Environment Engineering and Research. Dunedin, New Zealand, pp. 211–217.

Toyota, T., Haas, C., Tamura, T., 2011. Size distribution and shape properties of relatively small sea-ice floes in the Antarctic marginal ice zone in late winter. Deep-Sea Res. II 58 (9–10), 1182–1193.

Toyota, T., Takatsuji, S., Nakayama, M., 2006. Characteristics of sea ice floe size distribution in the seasonal ice zone. Geophys. Res. Lett. 33 (L02616).

Vaughan, G. L., Squire, V. A., 2011. Wave induced fracture probabilities for arctic sea-ice. Cold Regions Sci. Tech. 67 (1–2), 31–36.

Wadhams, P., Squire, V. A., Goodman, D. J., Cowan, A. M., Moore, S. C., 1988. The attenuation rates of ocean waves in the marginal ice zone. J. Geophys. Res. 93 (C6), 6799 – 6818.

WAMDI Group, 1988. The WAM model—A third generation ocean wave prediction model. J. Phys. Oceanogr. 18, 1775–1810.

Wang, R., Shen, H. H., 2011a. A continuum model for the linear wave propagation in ice-covered oceans: An approximate solution. Ocean Modelling 38, 244–250.

Wang, R., Shen, H. H., 2011b. Gravity waves propagating into an ice-covered ocean: A viscoelastic model. J. Geophys. Res. 115 (C06024, doi:10.1029/2009JC005591).

Weber, J. E., 1987. Wave attenuation and wave drift in the marginal ice zone. J. Phys. Oceanogr. 17, 2351–2361.

Weeks, W. F., Tucker, W. B., Frank, M., Fungcharoen, S., 1980. Characteristics of surface roughness and floe geometry of sea ice over the continental shelves of the Beaufort and Chukchi Seas. In: Pritchard, R. S. (Ed.), Sea ice processes and models. University of Washington Press, Seatle, pp. 300–312.

Williams, T. D., Bennetts, L. G., Squire, V. A., Dumont, D., Bertino, L., submitted. Wave-ice interactions in the marginal ice zone. Part 2: Numerical implementation and sensitivity studies along 1D transects of the ocean surface. Ocean Modelling.

Williams, T. D., Porter, R., 2009. The effect of submergence on the scattering by the interface between two semi-infinite sheets. Journal of Fluids and Structures 25, 777–793.

World Meteorological Organization, 1998. Guide to Wave Forecasting and Analysis, 2nd Edition. WMO No. 702. World Meteorological Organization.

Appendix A. Thin elastic plate model with the inclusion of damping

In this appendix we present the physical basis behind the dispersion relation of Robinson and Palmer (1990) (hereafter denoted RP90), which is derived by adding a damping coefficient to the usual thin elastic plate equation. Let $z = 0$ be the mean position of the ice-water interface and let $z = \eta_{\rm ice}$ be the position of the interface (the z coordinate axis points upwards, and the single horizontal coordinate axis, the x-axis, points to the right). We assume that $\eta_{\rm ice}$ is small enough that we can linearise about $z = 0$. In the formulation of RP90, the thin plate equation is modified to:

$$\Big(F\partial_x^4 + \rho_{\rm ice} h\partial_t^2\Big)\eta_{\rm ice} = P\Big|_{z=\eta_{\rm ice}} - \Gamma\partial_t\eta_{\rm ice}, \tag{A.1}$$

where F is the flexural rigidity of the plate, $\rho_{\rm ice}$ is the ice density, h is the ice thickness, Γ is the damping coefficient and P is the water pressure. The parameter Γ contributes to a drag pressure $(-\Gamma\partial_t\eta)$ that is proportional to the particle velocity—this is usually absent from the thin plate formulation. The rigidity is given by $F = Y^*h^3/12(1-\nu^2)$, where Y^* is the effective Young's Modulus (see §4.3) and $\nu = 0.3$ is the Poisson's ratio.

If we assume that the water is inviscid and incompressible and its flow is irrotational we can write the fluid particle velocity as $\mathbf{u} = (u, w)^T = \nabla\phi$, where $\nabla = (\partial_x, \partial_z)^T$. The pressure P is related to ϕ through the linearized Bernoulli equation, and ϕ satisfies Laplace's equation (incompressibility) and the sea floor condition for infinitely deep water:

$$P - P_{\rm atm} = -\rho\big(gz + \partial_t\phi\big), \tag{A.2a}$$

$$\nabla^2\phi = 0, \tag{A.2b}$$

$$\lim_{z\to-\infty}\partial_z\phi(x,z,t) = 0, \tag{A.2c}$$

where $P_{\rm atm}$ is the atmospheric pressure, $\rho = 1025\,\mathrm{kg\,m^{-3}}$ is the water density and $g = 9.81\,\mathrm{m\,s^{-2}}$ is the gravitational acceleration. We also need to apply a (linearized) kinematic condition at the surface:

$$\partial_t\eta_{\rm ice} = w(x,\eta_{\rm ice},t) \approx w(x,0) = \partial_z\phi(x,0,t). \tag{A.3}$$

Thus

$$\begin{aligned}\partial_t P\Big|_{z=\eta_{\rm ice}} &= -\rho\partial_t\Big(g\eta_{\rm ice} + \partial_t\phi(x,\eta_{\rm ice},t)\Big)\\ &\approx -\rho\Big(g\partial_z + \partial_t^2\Big)\phi(x,0,t),\end{aligned} \tag{A.4}$$

which, when combined with the time-derivative of (A.1), implies that

$$\big(F\partial_x^4 + \rho(g - d\partial_t^2) + \Gamma\partial_t\big)\partial_z\phi(x,0,t) = -\rho\partial_t^2\phi(x,0,t), \tag{A.5}$$

where $d = \rho_{\rm ice}h/\rho = 0.9h$ is the draft of the ice.

We now look for harmonic waves that obey (A.3) and (A.5) when the water depth is infinite:

$$\eta_{\text{ice}}(x,t) = \text{Re}\left[A_{\text{ice}}\mathrm{e}^{\mathrm{i}(\kappa x-\omega t)}\right], \tag{A.6a}$$

$$\phi(x,z,t) = \text{Re}\left[A_{\text{ice}}\frac{\omega}{\mathrm{i}\kappa}\mathrm{e}^{\mathrm{i}(\kappa x-\omega t)+\kappa z}\right], \tag{A.6b}$$

where A_{ice} is the amplitude of the ice displacement, $\omega = 2\pi/T$ is the radial frequency (T is the wave period), and κ is a complex wavenumber. A non-zero amplitude is only possible if κ satisfies the dispersion relation of RP90:

$$\big(F\kappa^4 + \rho(g - d\omega^2) - \mathrm{i}\omega\Gamma\big)\kappa = \rho\omega^2. \tag{A.7}$$

When $\Gamma = 0$, the primary root of interest, which we denote k_{ice}, is positive and real. For non-zero Γ, we denote the root closest to k_{ice} by $\mathcal{K}(\omega,\Gamma) = \tilde{k}_{\text{ice}} + \mathrm{i}\delta$, where $\tilde{k}_{\text{ice}}, \delta > 0$. For physical ranges of Γ ($\Gamma \lesssim 15\,\mathrm{Pa\,s\,m^{-1}}$) this is a unique choice, and $k_{\text{ice}} = \mathcal{K}(\omega, 0)$.

To give us some idea of the important non-dimensional quantities we can let $L^5 = F/(\rho\omega^2)$, and $\bar{\kappa} = \kappa L$. This turns (A.7) into

$$\big(\bar{\kappa}^4 + (a - \mathrm{i}b)\big)\bar{\kappa} = 1, \tag{A.8}$$

where

$$a = \frac{g}{L\omega^2} - \frac{d}{L}, \quad b = \frac{\Gamma}{\rho\omega L} = \frac{\Gamma}{\rho^{0.8}\omega^{0.6}F^{0.2}}.$$

The non-dimensional viscosity parameter b, which is $O(10^{-4})$ for higher frequencies, but is slightly bigger ($O(10^{-3})$) for lower frequencies, measures the importance of the damping effects. As well as decreasing with frequency, it also decreases with thickness (h) through the rigidity F.

Some asymptotic analysis shows that:

$$\mathcal{K}(\omega,\Gamma) = k_{\text{ice}}\left(1 + \frac{\mathrm{i}b(k_{\text{ice}}L)}{4(k_{\text{ice}}L)^5 + 1}\right) + O(b^2),$$

so effectively $\tilde{k}_{\text{ice}} \approx k_{\text{ice}}$. Also δ is approximately $O(10^{-8}\,\mathrm{m}^{-1})$ for higher frequencies but increases to $O(10^{-6}\,\mathrm{m}^{-1})$ for smaller frequencies. Therefore the effects of Γ can be neglected for small scale calculations such as the estimation of the strain in a single floe, or the reflection by a single ice edge. However, it is important in large scale calculations such as the attenuation by a large number of floes, so δ needs to be included to produce enough attenuation of long waves (Bennetts and Squire, 2012b).

Appendix B. The WIM of Dumont et al. (2011)

Appendix B.1. Amplitude spectrum

Dumont et al. (2011) (hereafter called DKB) considered small frequency intervals, $\Delta\omega$ wide, and set

$$\frac{1}{2}\mathscr{A}^2(\omega) = \int_{\omega-\frac{1}{2}\Delta\omega}^{\omega+\frac{1}{2}\Delta\omega} S(\omega')\mathrm{d}\omega' \approx \Delta\omega S(\omega). \tag{B.1}$$

This was based on the arguments that wave groups around the central frequency would separate as they traveled into the ice due to dispersion, and so the different wave groups would not interfere with each other. It was partly done in response to the numerical issue that ocean spectra produced by external wave models, if they weren't given parametrically, would only be given at discrete values.

However, approximation (B.1) has the fundamental flaw that, as the frequency resolution tends to zero, $\Delta\omega \to 0$, the amplitude also tends to zero, $\mathscr{A} \to 0$. Therefore, as a rough approximation, $\Delta\omega$ was replaced by ω, i.e.

$$S = \frac{1}{2\omega}\mathscr{A}^2. \tag{B.2}$$

This clearly causes problems when ω is significantly higher than $\Delta\omega$. However, we resolve the issue of the frequency resolution by considering numerical integrals of S which actually converge better as $\Delta\omega \to 0$.

Appendix B.2. Energy transport

Substituting (B.2) into the energy balance equation for waves in the MIZ (2) gives

$$\frac{1}{c_{\mathrm{g}}}D_t\mathscr{A} = -\frac{\hat{\alpha}}{2}\mathscr{A}. \tag{B.3}$$

This is the continuous version of the equation used by DKB to advect wave energy, so the two equations are equivalent. However, advecting S is more natural since it adds linearly, unlike $\mathscr{A}$.

Appendix B.3. Breaking criterion

The breaking criterion used by DKB in connection with the amplitude spectrum (B.2) was that the ice would break if $\mathscr{A}(\omega) > A_{\mathrm{c}}(\omega)$ where A_{c} was a critical wave amplitude, applied for any of the frequencies in the range appropriate to water waves. As mentioned above, this assumed wave groups would separate in the ice, and does not allow for the possibility of constructive interference between waves of different frequencies. By integrating S over all frequency space when determining the breaking probability of §3.2, we allow for the latter possibility implicitly.

The value used for the critical amplitude A_{c} was $A_{\mathrm{c}} = \min\{A_{\mathrm{c}}^{\varepsilon}, A_{\mathrm{c}}^{\sigma}\}$. The condition $\mathscr{A}(\omega) > A_{\mathrm{c}}^{\varepsilon}$ represents one standard deviation in the strain for the wave group centered at frequency ω being greater than their breaking strain ε_{c}, while the condition $\mathscr{A}(\omega) > A_{\mathrm{c}}^{\sigma}$ represents one standard deviation in the stress being greater than the flexural strength σ_{c}. Our breaking criterion applies the strain criterion in a different way (in order to allow for constructive interference, as discussed above), but we do not apply a stress criterion.

The method used by DKB to estimate the stress was intended to allow for the effects of cavitation and wetting. During cavitation, the ice floe does not follow the wave profile exactly and potentially causes a strong localized stress on the floe. However, the criterion predicts greater stress when the waves are longer than when they are shorter. This is unphysical in this regime as ice is relatively unaffected by long waves because of their low slope/curvature, normally small amplitude, and the low velocities they force surface objects to move at. As long waves also experience the least attenuation in the presence of ice cover, the stress criterion results in an unphysically wide MIZ. As a result, our parameterization does not invoke the stress criterion of DKB. However, a different method of allowing for cavitation and wetting could still be considered in the future.

We also note that Marchenko et al. (2011) derived an ice breakage criterion based on measured sea floor water pressure during an observed breakage event. Breakage was attributed to an increase in wave amplitudes (and hence stress and strain) produced by shoaling, so that the ice would break if the water depth H was less than a certain critical depth. This critical depth agrees with the one calculated using our method (adjusted for shallow water instead of infinitely deep water) to within reasonable uncertainty limits ($\sim 11\%$).

Appendix B.3.1. Fatigue

The discussion of the anelastic response of sea ice in §4.3 does not preclude the possibility that floes can gradually fatigue due to repeated bending imposed by passing waves. Fatigue, whether of the high-cycle type associated with elastic behavior and growth of microscopic cracks that eventually reach a critical size for fracture, or low cycle fatigue where the stress is sufficient for plastic deformation, is characterized by cumulative damage such that materials do not recover when rested, i.e. they behave inelastically as opposed to anelastically. Accordingly, the effective modulus approach described above, which includes only fully recoverable elastic deformation, cannot accommodate fatigue. There is, however, a suggestion (Langhorne et al., 1998) that an endurance limit, i.e. a value of stress for which a material will retain its integrity even when subjected to an infinite number of load cycles, exists for sea ice. This value, 0.6, was determined on stationary shore fast sea ice in McMurdo Sound, Antarctica. DKB therefore reduced their flexural strength by a factor of 0.6. We, on the other hand, have chosen not to do this because (i) the ice and wave conditions change rapidly in the MIZ so, while a stress greater than $0.6\sigma_{\mathrm{c}}$ can cause failure in principle, it may still occur at a timescale that is well beyond that associated with the local dynamics (recall that the endurance limit is for infinite time), (ii) fatigue strictly negates the use of an effective modulus, as permanent irrecoverable damage is gradually done to the sea ice either by the nucleation and propagation of cracks or by secondary and tertiary creep, and (iii) the fast ice data of Langhorne et al. (1998) show considerable scatter, which is a common feature of fatigue experiments even for simple materials. We rest content, therefore, with the expression for Y^* defined in equation (25a), noting that fatigue can easily be added at a later point if results indicate that it plays a role.

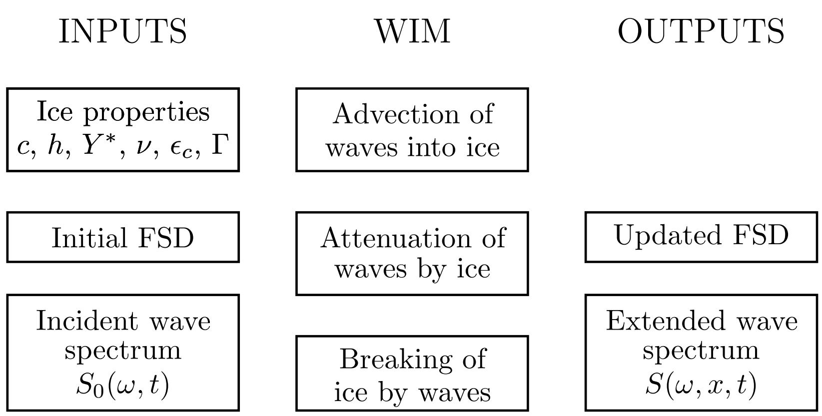

Figure B.1: The information flow in and out of the waves-in-ice model (WIM). An incident wave spectrum with density function $S_0(\omega, t)$ is prescribed at $x = 0$, where ω is the radial frequency (2π multiplied by the frequency), t is time, and x is the spatial variable. The ice properties shown as inputs—respectively the concentration, thickness, effective Young's modulus, Poisson's ratio and breaking strain of the ice, and the viscous damping parameter—combine with the initial floe size distribution (FSD) to affect the three components of the WIM itself: advection, attenuation and ice breakage. This results in the wave spectral density function $S(\omega, x, t)$ being extended into the ice (i.e. into the $x > 0$ region), and in the FSD changing.

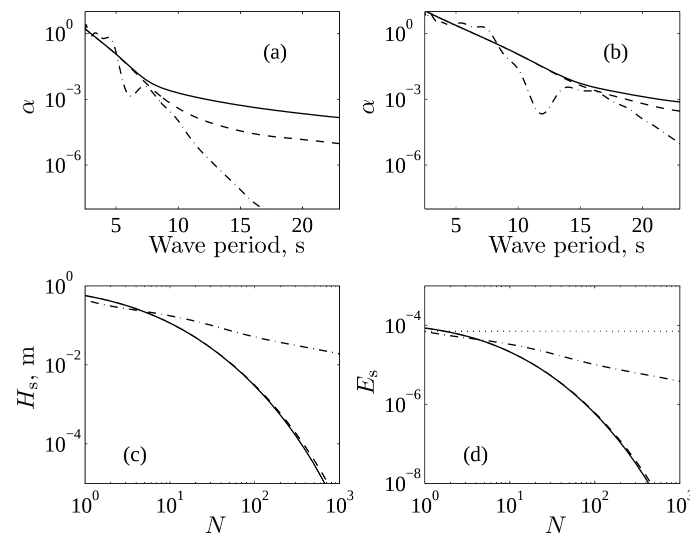

Figure B.2: Behavior of the different attenuation models (A: $- \cdot -$; B, $\Gamma = 0\,\mathrm{Pa\,s\,m^{-1}}$: $--$; B, $\Gamma = 13\,\mathrm{Pa\,s\,m^{-1}}$: $-$) (a, b): α is plotted against period for thicknesses 1 m (a) and 2 m (b). (c, d): The drop in H_s (c) and E_s (d) as a Bretschneider spectrum with peak period 7 s and initial H_s of 1 m travels past N floes of thickness 2 m. In (d), the strain that E_s must exceed to produce breaking, E_c, is plotted as a dotted line. (Here we have used $\varepsilon_c = 4.99 \times 10^{-5}$ and $\mathbb{P}_c = e^{-1}$, so $E_c = 7.06 \times 10^{-5}$.)

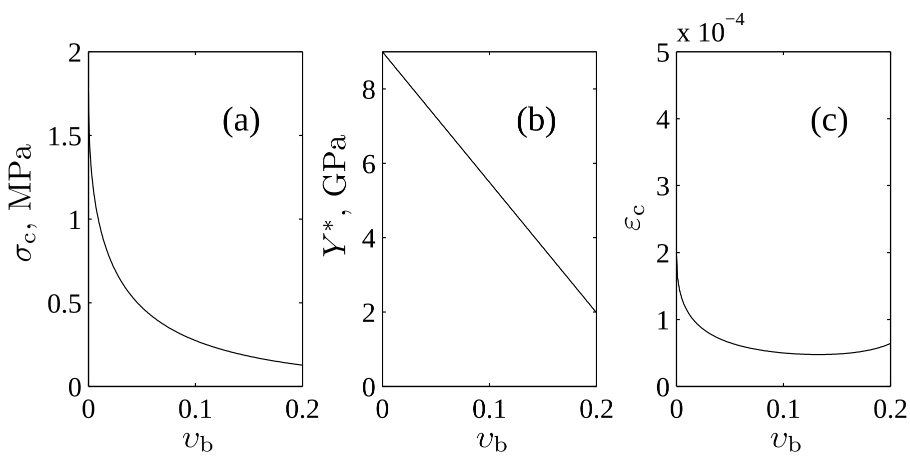

Figure B.3: Behavior of the flexural strength (a), and our models for the effective Young's modulus (b) and the breaking strain (c) with the brine volume fraction υ_b.